Inorg. Chem. **2008**, *47*, 8943−8956

Ligand-Derived Oxidase Activity. Catalytic Aerial Oxidation of Alcohols (Including Methanol) by Cu(II)-Diradical Complexes

Chandan Mukherjee, Ulrich Pieper, Eberhard Bothe, Vinzenz Bachler, Eckhard Bill, Thomas Weyhermüller, and Phalguni Chaudhuri*

Max-Planck-Institute for Bioinorganic Chemistry, Stiftstrasse 34-36, D-45470 Mülheim an der Ruhr, Germany

Received May 29, 2008

Seven new bis(o-iminosemiquinonato)copper(II) complexes, **1**−**5**, **1a**, **1b**, derived from differently substituted *N*-phenyl-2-aminophenol-based ligands, are described. Their crystal structures were determined by X-ray diffraction, and their electronic structures were established by various physical methods including electron paramagnetic resonance and variable-temperature (2−290 K) susceptibility measurements. Like complex **6**, which was reported recently by us, all complexes exhibit an $S_t = {}^1/_2$ ground state, based on the "isolated" copper(II)-spin character resulting from the dominating antiferromagnetic spin coupling between the two radicals; the ground-state electronic configuration can thus be designated as (↑↑↓)[R-Cu-R]. In addition, broken spin symmetry density functional solutions have been obtained. From the set of unrestricted canonical Kohn−Sham orbitals, the magnetic orbitals have been identified. The identification procedure is based on the nonvanishing overlap integrals between the space parts of orbitals occupied by electrons of opposite spin. The theoretically determined magnetic orbitals support the spin configurations suggested by the experiments. Electrochemical measurements (cyclic voltammetry and square-wave voltammetry) indicate ligand-centered redox processes. Complex **1** is found to be the best catalyst among the Cu(II) complexes for oxidation of primary alcohols with aerial oxygen as the sole oxidant to afford aldehydes under mild conditions. Thus, the function of the copper-containing enzyme Galactose Oxidase has been mimicked. Kinetic measurements in conjunction with electron paramagnetic resonance and electronic spectral studies have been used to decipher the catalytic oxidation process. A ligand-derived redox activity has been proposed as a mechanism for the aerial oxidation of primary alcohols.

Introduction

The presence of amino acid radicals[1] like tyrosine-based radicals as an electron reservoir in redox enzymes that activate dioxygen has stimulated model studies[2] with structurally defined small-molecule analogues of metallobiomolecules to elucidate the molecular basis of their reactivity. These model compounds have often the potential for being developed into new catalysts for oxygen activation that are capable of unusual substrate oxidations. In this regard the fungal enzyme galactose oxidase (GO), whose active site contains one copper ion coordinated to a tyrosyl (phenoxyl) radical and catalyzes the two-proton and two-electron oxidation of primary alcohols to the corresponding aldehydes in the presence of dioxygen, has stimulated important developments in the field of aerial oxidation of alcohols catalyzed by copper(II)-containing GO analogues.[2,3]

We and others have recently developed several GO-inspired catalytic systems,[2k,l,3−5] which efficiently aerobically oxidize alcohols to the corresponding aldehydes. Extensive kinetic and spectroscopic studies have been reported to support a GO mechanism: exclusive oxidation of primary alcohols.

While functional models of GO containing the Cu^{II}-phenoxyl moiety have been reported to catalyze the oxidation of primary alcohols including ethanol, the aerobic oxidation of methanol catalyzed by discrete copper(II) complexes is rare.[3c] Here we report a new mononuclear Cu(II) complex containing two monoanionic radical ligands which effectively catalyze the oxidation of methanol with dioxygen to formaldehyde.

* To whom correspondence should be addressed. E-mail: chaudh@mpi-muelheim.mpg.de.

(1) (a) Stubbe, J.; van der Donk, W. A. *Chem. Rev.* **1998**, *98*, 705. (b) Holm, R. H.; Kennepohl, P.; Solomon, E. I. *Chem. Rev.* **1996**, *96* (7), 2239. (c) Whittaker, J. W. *Chem. Rev.* **2003**, *103*, 2347. (d) Banerjee, R. *Chem. Rev.*; (Editorial); **2003**, *103*, 2081. (e) Chaudhuri, P.; Wieghardt, K. *Prog. Inorg. Chem.* **2001**, *50*, 151.

10.1021/ic8009767 CCC: $40.75
Published on Web 08/28/2008

This work stems from our interest in redox-active ligands, based on *N*-phenyl-2-aminophenol,[6−8] which can coordinate to a metal ion not only in their deprotonated forms but also in their one-electron oxidized o-iminobenzosemiquinone (SQ) radical and two-electron oxidized o-iminobenzoquinone (BQ) closed-shell forms (Scheme 1).

In a series of papers we have recently shown that the neutral square-planar complexes $[M^{II}(L^{R\bullet}_{SQ})_2]^0$ (M^{II} = Cu,[7] Ni,[7] Pd[7,8]) contain two O,N-coordinated o-iminobenzosemiquinonato(1-) ligands, $[L^{R\bullet}_{SQ}]^{1-}$, and thus are diradicals in which the two radical ligands couple intramolecularly antiferromagnetically resulting in either $S_t = {}^1/_2$ for Cu(II) or $S_t = 0$ for Ni(II) and Pd(II). In contrast, in octahedral $[Cr^{III}(L^{R\bullet}_{SQ})_3]$,[9] $[Fe^{III}(L^{R\bullet}_{SQ})_3]$,[9,12,14] $[Co^{III}(L^{R\bullet}_{SQ})_3]$,[10,11] and $[Ga^{III}(L^{R\bullet}_{SQ})_3]$[11] the three radical ligands couple depending on the metal center either ferromagnetically or antiferromagnetically. The substituent R on the aniline ring also has a profound influence on the nature of the exchange coupling.[11]

Scheme 1

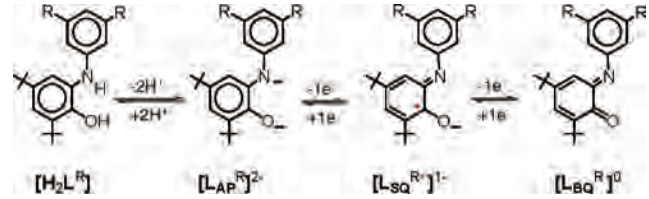

Scheme 2

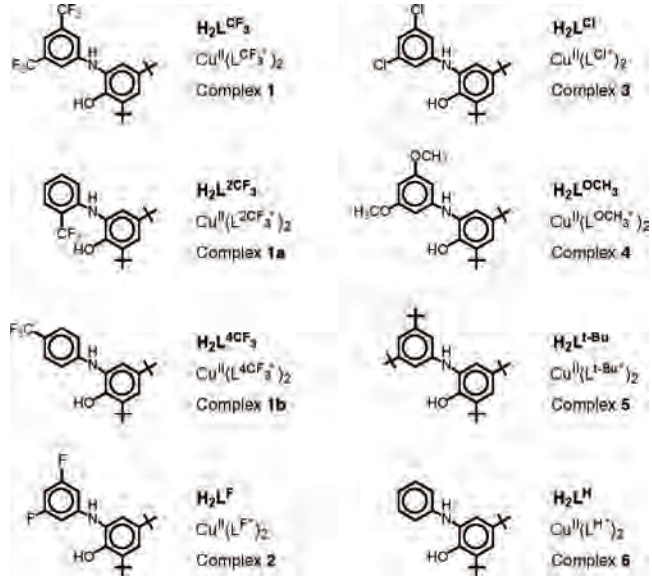

In the case of manganese[9,13] and vanadium[9] complexes, all three forms of the ligand $[HL^R_{AP}]^{1-}$, $[L^R_{AP}]^{2-}$ and $[L^{R\bullet}_{SQ}]^{1-}$ are present. The neutral iminobenzoquinone form $[L^R_{BQ}]^0$ does not appear so often.[6d,8]

The aim of our investigations of radical-containing metal complexes, with their oxidative catalytic activities toward different organic substrates in the presence of molecular oxygen as the sole oxidant, is to explore the aerial-oxidation chemistry of well-characterized metal complexes, which is expected to provide the basis for new catalytic oxidation systems for synthetic and industrial processes. Additionally, in such complexes containing redox-active "non-innocent" ligands, the multielectron redox activity may be entirely ligand-based,[4,6a,13a] which is largely unexplored for redox transformations of small molecules, for example, for oxidase-like reactivity. In this work we extend our previous study of Cu(II)-biradical systems[7] to various 3,5-substituted 2-anilinophenol ligands together with the GO-activity of radical-containing copper(II) complexes with the ligands listed in Scheme 2.

Experimental Section

Materials and Physical Measurements. Reagent- or analytical-grade materials were obtained from commercial suppliers and used without further purification, except those for electrochemical measurements. Elemental analyses (C, H, N, and metal) were performed by the Microanalytical Laboratory, Mülheim, Germany. Fourier-transform IR spectra of the samples in KBr disks were recorded with a Perkin-Elmer 2000 FT-IR instrument. Electronic absorption spectra in solution were measured with a Perkin-Elmer

(2) See for example: (a) Holm, R. H.; Solomon, E. I. *Chem. Rev.*; (Editorial); **2004**, *104*(2), 347. (b) Jazdzewski, B. A.; Tolman, W. B. *Coord. Chem. Rev.* **2000**, *200−202*, 633. (c) Mahadevan, V.; Klein Gebbink, R. J. M.; Stack, T. D. P. *Curr. Opin. Chem. Biol.* **2000**, *4*, 228. (d) Wang, Y.; Dubois, J. L.; Hedman, B.; Hodgson, K. O.; Stack, T. D. P. *Science* **1998**, *279*, 537. (e) Michel, F.; Thomas, F.; Hamman, S.; Saint-Aman, E.; Bucher, C.; Pierre, J.-L. *Chem.—Eur. J.* **2004**, *10*, 4115. (f) Itoh, S.; Taki, M.; Fukuzumi, S. *Coord. Chem. Rev.* **2000**, *198*, 3. (g) Benisvy, L.; Blake, A. J.; Collison, D.; Davies, E. S.; Garner, C. D.; McInnes, E. J. L.; McMaster, J.; Whittacker, G.; Wilson, C. *Chem. Commun.* **2001**, 1824. (h) Sokolowski, A.; Leutbecher, H.; Weyhermüller, T.; Schnepf, R.; Bothe, E.; Bill, E.; Hildebrandt, P.; Wieghardt, K. *J. Biol. Inorg. Chem.* **1997**, *2*, 444. (i) Pratt, R. C.; Stack, T. D. P. *Inorg. Chem.* **2005**, *44*, 2367; and references cited therein. (j) Taki, M.; Kumei, H.; Itoh, S.; Fukuzumi, S. *J. Inorg. Biochem.* **2000**, *78*, 1. (k) Thomas, F.; Gellon, G.; Gautier-Luneau, I.; Saint-Aman, E.; Pierre, J.-L. *Angew. Chem., Int. Ed.* **2002**, *41*, 3047. (l) Wang, Y.; Stack, T. D. P. *J. Am. Chem. Soc.* **1996**, *118*, 13097.
(3) (a) Chaudhuri, P.; Hess, M.; Flörke, U.; Wieghardt, K. *Angew. Chem., Int. Ed.* **1998**, *37*, 2217. (b) Chaudhuri, P.; Hess, M.; Weyhermüller, T.; Wieghardt, K. *Angew. Chem., Int. Ed.* **1999**, *38*, 1095. (c) Chaudhuri, P.; Hess, M.; Müller, J.; Hildenbrand, K.; Bill, E.; Weyhermüller, T.; Wieghardt, K. *J. Am. Chem. Soc.* **1999**, *121*, 9599.
(4) Chaudhuri, P.; Wieghardt, K.; Weyhermüller, T.; Paine, T. K.; Mukherjee, S.; Mukherjee, C. *Biol. Chem.* **2005**, *386*, 1023; and references therein.
(5) Paine, T. K.; Weyhermüller, T.; Wieghardt, K.; Chaudhuri, P. *Dalton Trans.* **2004**, 2092.
(6) (a) Mukherjee, C.; Weyhermüller, T.; Bothe, E.; Chaudhuri, P. *C. R. Acad. Sci., Ser. IIc: Chim.* **2007**, *10*, 313. (b) Mukherjee, C.; Weyhermüller, T.; Wieghardt, K.; Chaudhuri, P. *Dalton Trans.* **2006**, 2169. (c) Mukherjee, C.; Weyhermüller, T.; Bothe, E.; Rentschler, E.; Chaudhuri, P. *Inorg. Chem.* **2007**, *46*, 9895. (d) Mukherjee, C.; Weyhermüller, T.; Bothe, E.; Chaudhhuri, P. *Inorg. Chem.* **2008**, *47*, 2740.
(7) Chaudhuri, P.; Verani, C. N.; Bill, E.; Bothe, E.; Weyhermüller, T.; Wieghardt, K. *J. Am. Chem. Soc.* **2001**, *123*, 2213.
(8) Kokatam, S.; Weyhermüller, T.; Bothe, E.; Chaudhuri, P.; Wieghardt, K. *Inorg. Chem.* **2005**, *44*, 3709; and references therein.
(9) (a) Chun, H.; Verani, C. N.; Chaudhuri, P.; Bothe, E.; Bill, E.; Weyhermüller, T.; Wieghardt, K. *Inorg. Chem.* **2001**, *40*, 4157. (b) Chun, H.; Chaudhuri, P.; Weyhermüller, T.; Wieghardt, K. *Inorg. Chem.* **2002**, *41*, 790.
(10) Verani, C. N.; Gallert, S.; Bill, E.; Weyhermüller, T.; Wieghardt, K.; Chaudhuri, P. *Chem. Commun.* **1999**, 1747.
(11) Chaudhuri, P.; Wagner, R.; Pieper, U.; Biswas, B.; Weyhermüller, T. *Dalton Trans.* **2008**, 1286.
(12) Mukherjee, S.; Weyhermüller, T.; Bill, E.; Wieghardt, K.; Chaudhuri, P. *Inorg. Chem.* **2005**, *44*, 7099.
(13) (a) Mukherjee, S.; Weyhermüller, T.; Bothe, E.; Wieghardt, K.; Chaudhuri, P. *Dalton Trans.* **2004**, 3842. (b) Mukherjee, S.; Rentschler, E.; Weyhermüller, T.; Wieghardt, K.; Chaudhuri, P. *Chem. Commun.* **2003**, 1828.
(14) Mukherjee, S.; Weyhermüller, T.; Wieghardt, K.; Chaudhuri, P. *Dalton Trans.* **2003**, 3483.

Lambda 19 spectrophotometer. Magnetic susceptibilities of powdered samples were recorded with a superconducting quantum interference device (SQUID) magnetometer in the temperature range of 2−290 K with an applied field of 1 T. Experimental susceptibility data were corrected for the underlying diamagnetism using Pascal's constants and for the temperature-independent paramagnetism contributions. Mass spectra were recorded with either a Finnigan MAT 8200 (electron ionization, EIMS) or a MAT 95 (electrospray, ESI-MS) instrument. A Bruker DRX 400 instrument was used for NMR spectroscopy. X-band electron paramagnetic resonance (EPR) spectra were recorded with a Bruker ELEXSYS E500 spectrometer equipped with a helium flow cryostat (Oxford Instruments ESR 910). Cyclic voltammograms (CVs) were recorded using a conventional three-electrode arrangement, consisting of a glassy-carbon working electrode (of 2 mm diameter), an Ag/Ag^+ (0.01 M $AgNO_3$) reference electrode, and a Pt-wire counter electrode. Small amounts of ferrocene were added as an internal standard after completion of an experiment, and potentials are referenced versus the ferrocenium/ferrocene (Fc^+/Fc) couple. Potential control was achieved using an EG&G potentiostat/galvanostat (model 273A) with M270 software, and solutions of the complexes in CH_2Cl_2 containing 0.2 M $[(n\text{-}Bu)_4N]PF_6$ as supporting electrolyte were employed throughout.

Controlled-potential electrolysis at an appropriate fixed potential was performed at −25 °C in a jacketed quartz cell with the same type of reference electrode, a Pt-mesh working electrode, and a Pt-brush counter electrode. The cell (optical path length 0.5 cm) was mounted directly in a spectrophotometer (Hewlett-Packard HP 8453), allowing us to record UV−vis spectra in situ during electrolysis. After the completion of electrolysis, samples of the electrolyzed solutions were taken and rapidly frozen by liquid nitrogen for EPR analysis.

Preparation of the Ligands H_2L^R (R = −H,[7] $-OCH_3$,[11,15] −t-Bu,[13] $-CF_3$,[8,13] −F,[12] −Cl[7]). The ligands were prepared according to the procedures described earlier in the literature.[7,8,11−13,15]

Preparation of Complexes $[Cu^{II}(L^{R\bullet})_2]$. As the $Cu^{II}(L^{R\bullet})_2$ complexes were prepared by a similar protocol, a representative method is only described. A solution containing H_2L^R (2 mmol), $[Cu^I(CH_3CN)_4]ClO_4$ (0.655 g; 2 mmol) and triethylamine (0.2 mL) in acetonitrile (30 mL) was stirred at ambient temperature for 2 h in the presence of air to yield a dark green suspension. The microcrystalline green solid was collected by filtration and air-dried. The compounds were recrystallized from a CH_3CN/CH_2Cl_2 mixture (1:1) by slow evaporation. The yields were in the range 60−70% based on the starting ligand.

The same material is also obtained by the reaction of CuCl with the corresponding ligand in methanol in the presence of the base Et_3N.

Complex 1, $[Cu^{II}(L^{CF_3\bullet})_2]$. Anal. Calcd for $C_{44}H_{46}F_{12}N_2O_2Cu$: C, 57.05; H, 5.0; N, 3.02; Cu, 6.86. Found: C, 57.2; H, 5.0; N, 3.1; Cu, 6.8. EI-MS: *m/z* 925 (100%), 926 (67.3%), 927 (67.94%), 928 (16.18%) $[M]^+$. IR(KBr, cm^{-1}): 2958−2874, 1655, 1585, 1467, 1381, 1367, 1280, 1175, 1132, 1105, 1032, 1005, 952, 890, 683.

Complex 1a, $[Cu^{II}(L^{2CF_3\bullet})_2]$. Anal. Calcd for $C_{44}H_{51}F_6N_3O_2Cu$: C, 63.56; H, 6.18; N, 5.05; Cu, 7.64. Found: C, 63.7; H, 6.2; N, 5.0; Cu, 7.9. ESI-MS(+) *m/z* 789.4 (100%) $[M]^+$. IR(KBr, cm^{-1}): 2957−2869, 1600, 1577, 1487, 1463, 1387, 1360, 1334, 1316, 1254, 1181, 1167, 1156, 1131, 1110, 1057, 1034, 994, 862, 852, 759, 650.

Complex 1b, $[Cu^{II}(L^{4CF_3\bullet})_2]$. Anal. Calcd for $C_{42}H_{48}F_6N_2O_2Cu$: C, 63.82; H, 6.12; N, 3.54; Cu, 8.04. Found: C, 63.8; H, 6.1; N, 3.6; Cu, 8.0. EI-MS(+): *m/z* 789.6 (100%) $[M]^+$. IR(KBr, cm^{-1}): 2964−2871, 1609, 1583, 1464, 1323, 1258, 1163, 1125, 1103, 1065, 1016, 891, 856, 841, 776, 627.

Complex 2, $[Cu^{II}(L^{F\bullet})_2]$. Anal. Calcd for $C_{40}H_{46}F_4N_2O_2Cu$: C, 66.14; H, 6.38; N, 3.86; Cu, 8.75. Found: C, 66.0; H, 6.4; N, 3.8; Cu, 8.9. EI-MS: *m/z* 725 (100%) $[M]^+$. IR(KBr, cm^{-1}): 2961−2890, 1612, 1591, 1522, 1467, 1446, 1419, 1340, 1249, 1115, 1137, 990, 870, 829, 775, 678, 658.

Complex 3, $[Cu^{II}(L^{Cl\bullet})_2]$. Anal. Calcd for $C_{40}H_{46}Cl_4N_2O_2Cu$: C, 60.65; H, 5.85; N, 3.54; Cu, 8.02. Found: C, 60.9; H, 5.8; N, 3.5; Cu, 8.2. EI-MS: *m/z* 791 (18%) $[M]^+$, 571 (30%), 556(40%), 365(100%). IR(KBr, cm^{-1}): 2953−1866, 1647, 1568, 1558, 1463, 1413, 1384, 1332, 1253, 1105, 1034, 1001, 940, 851, 800, 763, 678, 648.

Complex 4, $[Cu^{II}(L^{OCH_3\bullet})]$. Anal. Calcd for $C_{44}H_{58}N_2O_6Cu$: C, 68.23; H, 7.55; N, 3.62; Cu, 8.21. Found: C, 68.1; H, 7.6; N, 3.6; Cu, 8.0. EI-MS: *m/z*, 773 (85.2%), 774(52%), 775(54.7%), 776(27%) $[M]^+$, 354(31.3%), 355(100%), 356(35.3%), 357(54%) $[M\text{-}L^{OCH_3}]^+$. IR(KBr, cm^{-1}): 2950−2867, 1600, 1584, 1515, 1471, 1416, 1337, 1316, 1247, 1197, 1156, 1143, 1064, 955, 941, 855, 813, 775, 683, 645.

Complex 5, $[Cu^{II}(L^{t\text{-}Bu\bullet})_2]$. The compound was recrystallized from a $CH_3OH/(C_2H_5)_2O$ solvent mixture (1:1) to obtain X-ray quality crystals. Anal. Calcd for $C_{56}H_{82}N_2O_2Cu\cdot(C_2H_5)_2O$: C, 75.62; H, 9.73; N, 2.94; Cu, 6.67. Found: C, 75.0; H, 9.8; N, 3.0; Cu, 6.8. EI-MS: *m/z* 877(100%), 878(78.8%), 879(75.9%), 880(43.8%), 881(16.5%) $[M^+]^+$, 470(21.1%) $[M\text{-}L^{t\text{-}Bu}]^+$, 350(53.3%) $[L^{t\text{-}Bu}\text{-}C_4H_9]^+$. IR(KBr, cm^{-1}): 2961−2868, 1593, 1581, 1527, 1516, 1478, 1463, 1416, 1392, 1386, 1362, 1297, 1268, 1248, 1119, 1109, 1038, 1005, 958, 875, 855, 706.

Complex 6 $[Cu^{II}(L^{H\bullet})_2]$. The complex has been reported in ref 7.

Preparation of $[^nBu_4N][OCD_3]$. To a suspension of metallic potassium (1.07 g; 27.4 mmol) in dry toluene (30 mL) was added CD_3OD (4.5 mL; 114 mmol). The resulting suspension was stirred for 8 h till the complete dissolution of the metal. A fraction (4 mL) of the solution was taken out, to which was added *n*-tetrabutylammonium perchlorate (9.35 g; 27.4 mmol). Addition of dry ether initiated precipitation of $KClO_4$ and $[^nBu_4N]ClO_4$, which were filtered out under argon, and the filtrate was evaporated to dryness to collect $[^nBu_4N][OCD_3]$.

Procedure for the Oxidation of Benzylalcohol and Determination of the Concentration of Benzaldehyde. A solution of 5×10^{-4} M of the copper(II)-radical complex (catalyst), 5×10^{-2} M benzyl alcohol and 4.5×10^{-2} M tetrabutylammonium methoxide in 20 mL of dichloromethane was made and stirred for 15 h in air for the oxidation. An aliquot of the solution was passed through a neutral Al_2O_3 column, and the concentration of benzaldehyde (product) was determined from LC measurements, which were performed on a HPLC instrumentation (Shimadzu) using a Gilson M305 pump, and the Diode-Array-Detector (DAD) SPDM 10AV. As eluent, a mixture of CH_3OH/H_2O (3:1) with a flow velocity of 0.8 mL/min through a Luna-5 C18 column was used.

Procedure for the Oxidation of Ethanol and Determination of the Concentration of Acetaldehyde. A solution of the catalyst (5×10^{-4} M) and tetrabutylammonium ethoxide (5×10^{-2} M) in dichloromethane (20 mL) was stirred in air for 3−5 h for the oxidation. An aliquot of 0.5 mL of catalytic solution was extracted with water (10 mL). The aqueous solution was analyzed for acetaldehyde by the 3-methyl-2-benzothiazolone hydrazone

(15) Chaudhuri, P.; Bill, E.; Wagner, R.; Pieper, U.; Biswas, B.; Weyhermüller, T. *Inorg. Chem.* **2008**, *47*, 5549.

reagent, as described in the literature[16] for spectrophotometric determination of water-soluble aldehydes. The absorption was measured at 635 and 670 nm against the blank.

Procedure for the Oxidation of Methanol and Determination of the Concentration of Formaldehyde. A solution of the catalyst (5×10^{-4} M) and tetrabutylammonium methoxide (5×10^{-2} M) in dichloromethane (20 mL) was stirred in air for the oxidation (~15 h). The produced formaldehyde was extracted into an aqueous phase (10 mL) from 0.5 mL of the catalytic solution. The aqueous solution (5 mL) was mixed with 5 mL of the Hantzsch reagent[17] and warmed at 60 °C for 5 min; the solution was cooled to room temperature before the absorption is measured at $\lambda = 414$ nm ($\varepsilon \sim 8000$ M^{-1} cm^{-1}) against the blank.

X-ray Crystallographic Data Collection and Refinement of the Structures 1−5. Single crystals of **1**−**5** were coated with perfluoropolyether, picked up with glass fibers, and mounted on a Nonius Kappa-CCD diffractometer equipped with a cryogenic nitrogen cold stream operating at 100(2) K. Graphite-monochromated Mo Kα radiation ($\lambda = 0.71073$ Å) was used. Final cell constants were obtained from a least-squares fit of all measured reflections. Intensity data were corrected for Lorentz and polarization effects. The data set for **2** were not corrected for absorption, whereas the intensity data sets for **1** and **5** were corrected for absorption with the program SADABS (version 2.1) and those for **1a**, **3**, and **4** with the use of Gaussian, face-indexed program. The Siemens ShelXTL software package[18] (Sheldrick, G. M., Universität Göttingen, Göttingen, Germany) was used for solution, refinement, and artwork of the structures; the neutral atom scattering factors of the program were used. Non-hydrogen atoms were refined anisotropically, and hydrogen atoms were placed at calculated positions and refined as riding atoms with isotropic displacement parameters. Details of data collection and structure refinements are summarized in Table 1.

Computational Methods and Theoretical Considerations. Program, Methods, and Basis Sets. All computations have been performed by means of the Gaussian 03 suite of ab initio programs.[19] To calculate complex **1** we applied density functional theory (DFT) in the B3LYP methodology.[20,21] For describing the copper atom, we employed the basis set as referenced by the

Table 1. Crystallographic Data for **1**, **1a**·CH_3CN, **2**, **3**, **4**, and **5**·$(C_2H_5)_2O$

	1	**1a**·CH_3CN	**2**	**3**	**4**	**5**·$(C_2H_5)_2O$
empirical formula	$C_{44}H_{46}CuF_{12}N_2O_2$	$C_{44}H_{51}CuF_6N_3O_2$	$C_{40}H_{46}CuF_4N_2O_2$	$C_{40}H_{46}Cl_4CuN_2O_2$	$C_{44}H_{58}CuN_2O_6$	$C_{60}H_{92}CuN_2O_3$
formula weight	926.37	831.42	726.33	792.13	774.46	952.90
temperature, K	100(2)	100(2)	100(2)	100(2)	100(2)	100(2)
wavelength (Mo Kα), Å	0.71073	0.71073	0.71073	0.71073	0.71073	0.71073
crystal system	triclinic	monoclinic	monoclinic	monoclinic	monoclinic	triclinic
space group	$P\bar{1}$	$P2_1/n$	$P2_1(1)/n$	$P2_1/c$	$P2_1$	$P\bar{1}$
unit cell dimensions	a = 11.426(1) Å,	a = 17.1824(3) Å,	a = 5.8867(5) Å,	a = 12.1419(8) Å,	a = 20.031(3) Å,	a = 9.5092(7) Å,
	b = 14.197(2) Å,	b = 11.8651(2) Å,	b = 17.533(2) Å,	b = 10.2848(6) Å,	b = 10.6339(9) Å,	b = 16.365(1) Å,
	c = 14.726(2) Å,	c = 21.0332(5) Å,	c = 17.854(2) Å,	c = 15.3145(10) Å,	c = 20.720(3) Å,	c = 19.024(1) Å,
	α = 67.95(2)°	α = 90.00°	α = 90.00°	α = 90.00°	α = 90.00°	α = 83.078(3)°
	β = 81.28(2)°	β = 101.50(4)°	β = 95.32(2)°	β = 92.543(4)°	β = 109.73(2)°	β = 79.902(3)°
	γ = 83.86(2)°	γ = 90.00°	γ = 90.00°	γ = 90.00°	γ = 90.00°	γ = 75.567(3)°
volume (Å^3), Z	2185.2(5), 2	4202(1), 4	1834.8(3), 2	1910.5(2), 2	4154.4(9), 4	2854.2(4), 2
density (calc.) Mg/m^3	1.408	1.314	1.315	1.377	1.238	1.109
absorption coeff, mm^{-1}	0.589	0.586	0.652	0.888	0.573	0.425
F(000)	954	1740	762	826	1652	1038
crystal size (mm)	0.36 × 0.16 × 0.15	0.4 × 0.28 × 0.2	0.32 × 0.21 × 0.14	0.33 × 0.22 × 0.16	0.50 × 0.40 × 0.16	0.30 × 0.19 × 0.14
reflections collected	17366	82338	36228	15776	35276	19197
independent reflect.	8175 [R(int) = 0.0368]	13340 [R(int) = 0.0448]	6617 [R(int) = 0.0889]	4265 [R(int) = 0.0498]	16419 [R(int) = 0.0448]	8051 [R(int) = 0.0378]
absorption correction	semiempirical from equiv.	Gaussian, face-indexed	not measured	Gaussian, face-indexed	Gaussian, face-indexed	SADABS
data/restraints/param.	8175/22/577	13340/0/518	6610/0/229	4249/0/229	16401/0/988	8044/0/624
goodness-of-fit on F^2	1.021	1.058	0.948	1.012	0.982	0.957
final R indices [$I > 2\sigma(I)$]	$R1$ = 0.0484, $wR2$ = 0.1076	$R1$ = 0.0385, $wR2$ = 0.0947	$R1$ = 0.0409, $wR2$ = 0.0870	$R1$ = 0.0380, $wR2$ = 0.0809	$R1$ = 0.0441, $wR2$ = 0.0871	$R1$ = 0.0391, $wR2$ = 0.0991
R indices (all data)	$R1$ = 0.0764, $wR2$ = 0.1193	$R1$ = 0.0461, $wR2$ = 0.0987	$R1$ = 0.0861, $wR2$ = 0.0991	$R1$ = 0.0719, $wR2$ = 0.0919	$R1$ = 0.0724, $wR2$ = 0.0959	$R1$ = 0.0644, $wR2$ = 0.1097
absolute structure parameter					0.502(9)	

(16) Sawicki, E.; Hauser, T. R.; Stanley, T. W.; Elbert, W. *Anal. Chem.* **1961**, *33*, 93.

(17) Nash, T. *Biochem.* **1953**, *55*, 416.

(18) (a) Sheldrick, G. M. *ShelXL97*; Universität Göttingen: Göttingen, Germany, 1997. (b) *SHELXTL*, version 6.14; Bruker AXS: Karlsruhe, Germany.

(19) Frisch, M. J.; Trucks, G. W.; Schlegel, H. B.; Scuseria, G. E.; Robb, M. A.; Cheeseman, J. R.; Montgomery, J. A., Jr.; Vreven, T.; Kudin, K. N.; Burant, J. C.; Millam, J. M.; Iyengar, S. S.; Tomasi, J.; Barone, V.; Mennucci, B.; Cossi, M.; Scalmani, G.; Rega, N.; Petersson, G. A.; Nakatsuji, H.; Hada, M.; Ehara, M.; Toyota, K.; Fukuda, R.; Hasegawa, J.; Ishida, M.; Nakajima, T.; Honda, Y.; Kitao, O.; Nakai, H.; Klene, M.; Li, X.; Knox, J. E.; Hratchian, H. P.; Cross, J. B.; Adamo, C.; Jaramillo, J.; Gomperts, R.; Stratmann, R. E.; Yazyev, O.; Austin, A. J.; Cammi, R.; Pomelli, C.; Ochterski, J. W.; Ayala, P. Y.; Morokuma, K.; Voth, G. A.; Salvador, P.; Dannenberg, J. J.; Zakrzewski, V. G.; Dapprich, S.; Daniels, A. D.; Strain, M. C.; Farkas, O.; Malick, D. K.; Rabuck, A. D.; Raghavachari, K.; Foresman, J. B.; Ortiz, J. V.; Cui, Q.; Baboul, A. G.; Clifford, S.; Cioslowski, J.; Stefanov, B. B.; Liu, G.; Liashenko, A.; Piskorz, P.; Komaromi, I.; Martin, R. L.; Fox, D. J.; Keith, T.; Al-Laham, M. A.; Peng, C. Y.; Nanayakkara, A.; Challacombe, M.; Gill, P. M. W.; Johnson, B.; Chen, W.; Wong, M. W.; Gonzalez, C.; Pople, J. A. *Gaussian03*, Revision C.01; Gaussian, Inc.: Wallingford, CT, 2004.

(20) (a) Becke, A. D. *Phys. Rev. A* **1988**, *38*, 3098. (b) Noodleman, L. *J. Chem. Phys.* **1981**, *74*, 5737. (c) Noodleman, L.; Davidson, E. R. *Chem. Phys.* **1986**, *109*, 131.

(21) (a) Lee, C.; Yang, W.; Parr, R. G. *Phys. Rev. B* **1988**, *37*, 735. (b) Miehlich, B.; Savin, A.; Stoll, H.; Preuss, H. *Chem. Phys. Lett.* **1989**, *157*, 200.

Gaussian 03 keyword SDD. This basis set simulates the Ne core by a pseudo potential and the valence atomic orbitals are described by means of a very flexible basis set.[22] For all ligand atoms of **1**, the 6−31g* basis sets[23] have been employed.

Broken Symmetry Electronic State. The electronic ground state of **1** is of doublet spin multiplicity ($S = {}^1/_2$). The temperature dependence of the magnetic susceptibility of **1** shows that a high spin quartet state is slightly above the electronic state. Therefore, a broken symmetry (BS) state is suggested for a description of the electronic ground state of **1**. To obtain the appropriate BS state, the following computational procedure has been applied. First, we computed the high spin quartet state ($S = {}^3/_2$) by using the unrestricted Kohn−Sham (UKS) approach in the unrestricted B3LYP (UB3LYP) DFT framework. Second, the stability of this UKS solution has been checked by means of the stability analysis[24] implemented in Gaussian 03. The UKS solution turned out to be stable. Third, the quartet high spin UKS orbitals have been used as starting orbitals for a computation of the doublet electronic ground state ($S = {}^1/_2$). Fourth, the UKS solution for the almost spin pure doublet ground state has been tested by means of the stability analysis.[19,24] The almost spin pure solution turned out to be unstable. The required wave function optimization (stable = "opt")[19] led to an UKS Slater determinant having an energy that is lower than the energy of the spin pure solution. This UKS Slater determinant produced an S^2-expectation value of about $\langle S^2\rangle = 1.7$. Thus, the BS DFT solution represents a mixture between a doublet ($\langle S^2\rangle = 0.75$) and a quartet ($\langle S^2\rangle = 3.75$) state. We optimized the geometry for the BS state by using the guess = "always" option of Gaussian 03.

Determination of Magnetic Orbitals. In the BS UKS DFT solution for **1**, the space parts of the α- and β-spin orbitals are orthonormal. Overlap integrals between the space parts of the α- and β-spin orbitals, however, are nonvanishing. This nonorthogonality combined with the concept of corresponding orbitals[25] has been used to define magnetic orbitals that are an ingredient of the BS formalism for the computation of exchange coupling constants.[26] We feel, however, that also standard canonical α- and β-MOs of an UKS Slater determinant might serve as magnetic orbitals. Overlap integrals between canonical α- and β-MOs may quantify the following notion. If the overlap integral between an occupied α- and an occupied β-MO is close to one, the two electrons (with opposite spin) in these MOs occupy the same region of space. Consequently, the two electron spins are strongly antiferromagnetically coupled. If the overlap integral is small, the two electrons occupy different regions of space and their spins are only weakly antiferromagnetically coupled. If an occupied α- (β)-MO overlaps preferentially with an unoccupied β- (α)-MO, the electron in the occupied α- (β)-MO remains unpaired. These considerations lead to two simple rules for determining magnetic orbitals: (i) If an occupied α- (β)-MO overlaps strongly with an unoccupied β- (α)-MO, the occupied α- (β)-MO is a magnetic orbital. (ii) If an occupied α- (β)-MO overlaps only weakly with the manifold of occupied β- (α)-MOs, the occupied α- (β)-MO is a magnetic orbital. A short computer program has been written that provides all overlap integrals in the sequence of decreasing magnitude.[27] This ordering facilitates the application of the two rules given above.

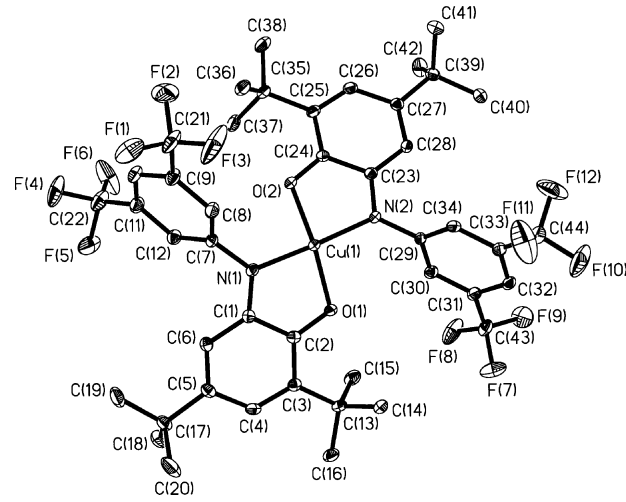

Figure 1. Oak Ridge Thermal Ellipsoid Plot (ORTEP) diagram of the neutral molecule **1**, with 50% probability of the ellipsoids.

Results and Discussion

The ligands are readily available in good yields from the reaction of 3,5-di-*tert*-butylcatechol and 3,5-disubstituted aniline in the presence of air and the base triethylamine. The reaction of the ligands with salts such as Cu^ICl, $[Cu^I(CH_3CN)_4]ClO_4$ in CH_3CN or CH_3OH in the presence of air affords dark green crystalline materials **1**−**5**. They are completely air-stable in the solid state and also in solution for a few days.

The IR spectra of **1**−**5** are very similar and do not warrant any special discussion, and the bands are given in the Experimental Section. A noticeable feature is the absence of the bands at ∼3410−3460 cm^{-1} and 3320−3350 cm^{-1} due to ν(OH) and ν(NH) vibrations, respectively, of the ligands in complexes **1**− **5**, indicating the absence of these protons in the coordinated ligands. EI-MS has been proven to be a very useful analytical tool for characterizing all complexes, which show the molecule-ion peak in most of the cases as the base peak (100%).

Description of the Structures. The crystal structures of complexes **1**, **1a**, **2**−**5** have been determined by single-crystal X-ray crystallography at 100(2) K. The X-ray structure of **6** has been reported earlier.[7] As the atom connectivity and the oxidation state of the ligands in **1**−**5** are identical, the molecular structure of **1**, $[Cu^{II}(L^{CF_3\bullet})_2]$ is only shown in Figure 1; the structures of **1a**, **2**−**5** are displayed in Supporting Information, Figures S1−S5. The geometry around the Cu(1) center is distorted square-planar N_2O_2, with two nitrogen donor atoms of the two $[L^{CF_3\bullet}]^-$ ligands always in the trans position with respect to each other (as are the two oxygen donors). The C−C bond distances for the rings with the CF_3-substituents in complex **1** have been found to lie within the range of 1.388 ± 0.010 Å, indicating that these C−C lengths are equidistant and the conjugation in the phenyl rings is retained. In contrast, the six C−C distances

(22) Preuss, H.; Stoll, H.; v. Szentpaly, L. *Chem. Phys. Lett.* **1989**, *89*, 418; the SDD basis set contraction scheme for the copper atom has been obtained from the log file as printed out by Gaussian 03.
(23) Hehre, W.; Ditchfield, J.; Pople, J. A. *J. Chem. Phys.* **1972**, *56*, 2257.
(24) Bauernschmitt, R.; Ahlrichs, R. *J. Chem. Phys.* **1996**, *104*, 9047.
(25) Neese, F. *J. Phys. Chem. Solids* **2004**, *65*, 781.
(26) See, for example, Caballol, R.; Castell, O.; Illas, F.; Moreira, I. de P. R.; Malrieu, J. P. *J. Phys. Chem. A* **1997**, *101*, 7860.
(27) This short FORTRAN program is available on request from the authors.

Table 2. Selected Bond Distances (Å) and Angles (degree) for **1**

Cu(1)−N(1)	1.925(2)	C(4)−C(5)	1.434(4)
Cu(1)−N(2)	1.929(2)	C(5)−C(6)	1.364(4)
Cu(1)−O(1)	1.932(2)	C(6)−C(1)	1.414(4)
Cu(1)−O(2)	1.932(2)	C(23)−N(2)	1.345(3)
C(2)−O(1)	1.300(3)	C(26)−C(27)	1.443(4)
C(1)−N(1)	1.342(3)	C(23)−C(24)	1.456(4)
C(2)−C(1)	1.457(4)	C(24)−C(25)	1.434(4)
C(1)−C(6)	1.414(4)	C(25)−C(26)	1.368(4)
C(3)−C(4)	1.369(4)	C(28)−C(27)	1.368(4)
C(7)−N(1)	1.415(4)	C(24)−O(2)	1.297(4)
C(8)−C(9)	1.385(4)	C(29-C(30)	1.390(4)
C(10)−C(9)	1.388(4)	C(30)−C(31)	1.387(4)
C(11)−C(10)	1.383(4)	C(31)−C(32)	1.394(4)
C(12)−C(11)	1.391(4)	C(32)−C(33)	1.382(4)
C(7)−C(12)	1.388(4)	C(33)−C(34)	1.402(4)
C(7)−C(8)	1.390(4)	C(29)−C(34)	1.381(5)
O(1)−Cu(1)−N(1)	83.84(8)	O(1)−Cu(1)−O(2)	162.27(10)
N(1)−Cu(1)−N(2)	174.98(10)	O(2)−Cu(1)−N(2)	83.62(9)
N(2)−Cu(1)−O(1)	99.62(11)	O(2)−Cu(1)−N(1)	94.19(9)
C(24)−O(2)−Cu(1)	111.2(2)	C(2)−O(1)−Cu(1)	111.8(2)
C(23)−N(2)−C(29)	119.9(2)	C(1)−N(1)−C(7)	123.0(2)
Cu(1)−N(2)−C(23)	112.9(2)	C(7)−N(1)−Cu(1)	122.5(2)
C(29)−N(2)−Cu(1)	127.1(2)	C(1)−N(1)−Cu(1)	113.0(2)

in the ring with C(1) to C(6) atoms or with C(23) to C(28) atoms are not equidistant: the typical pattern of the iminobenzosemiquinone radicals of a short, a long, and again a short bond and three adjacent long bonds is found. For example: C(3)−C(4) 1.369(4), C(4)−C(5) 1.434(4), C(5)−C(6) 1.364(4), C(6)−C(1) 1.414(4), C(1)−C(2) 1.457(4), C(2)−C(3) 1.432(4) Å. Thus, the rings with the *tert*-butyl groups adopt a quinoid-type structure. The coordination geometry around the nitrogen donors, N(1) and N(2), is planar indicating that these nitrogens are three-coordinate (sp^2 hybridization) and not protonated. Additionally, the bond lengths C(1)−N(1) and N(2)−C(23) at 1.343(3) and 1.345(3) Å, respectively, and C(2)−O(1) and C(24)−O(2) at 1.300(3) and 1.297(3) Å, respectively, are significantly shorter than the corresponding C−N and C−O bonds of order one, thus indicating the radical nature of the related phenyl rings. The geometrical parameters for **1** are identical within experimental error to those for the iminobenzosemiquinonate monoanionic radical ligands reported for **6** and other complexes in the literature.[6−15] Consequently, the metal ion Cu, can safely be assigned to the physical oxidation state +II. Table 2 lists the selected bond distances and angles for **1**.

For a comparison purpose, the dihedral angle between the planes comprising Cu(1)O(1)C(2)C(1)N(1) and Cu(1)O(2)C(24)C(23)N(2) atoms (Figure 1) in complex **1**, together with the corresponding angles for **1a**, **2**−**6**, are listed in Table 3. It is noteworthy, that in spite of the more bulky nature of the *tert*-butyl group than those for the other substituents, the dihedral angle for **5** is very close to that for **2**, **3**, and **6** and deviates significantly from those for **1** and **1a**. Thus, both of the operating effects, electronic and steric, are important for the distortion found in **1**−**6**.

Magnetochemistry and EPR Spectroscopy. The magnetic properties of complexes **1**−**5** were determined by variable-temperature (2−290 K) magnetic susceptibility (SQUID) measurements and EPR spectroscopy.

Like complex **6**, whose electronic ground state has been

Table 3. Dihedral Angles Between the Two Cu(II)-Planes in **1**−**6**

complexes	dihedral angle betweenthe Cu(II)-planes
1(−CF_3)	24.2°
1a($2CF_3$)	25.4°
2(−F)	0°
3(−Cl)	0°
4(−OMe)	8.4°
5(−^{t}Bu)	1.1°
6(−H)[a]	0°

[a] Reference 7.

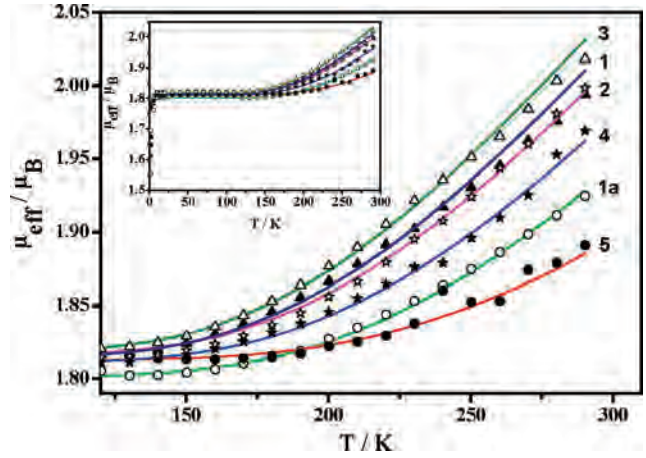

Figure 2. Plots of μ_{eff} vs T (>120 K) to emphasize the nesting for complexes **1**−**5**. (Inset) Plots of μ_{eff} vs T (2−290 K) for complexes **1**−**5**. The solid lines represent the best fits of the experimental data using $J = 0$ (fixed) (see text).

reported previously,[7] complexes **1**−**5** exhibit an $S_t = {}^1/_2$ ground state, as is evident from the temperature dependence of the effective magnetic moments for **1**−**5**, shown in Figure 2. At temperatures below ~120 K, a nearly constant value of $\mu_{eff} = 1.81 \pm 0.01\ \mu B$ is observed for all complexes. The effective magnetic moment increases monotonically but with different slopes above ~120 K indicating population of the excited states with higher spin multiplicity than 2. As complexes **1**−**5**, like **6**, are three-spin molecules with spins of two radicals ($S_{R1} = S_{R2} = {}^1/_2$) and one Cu(II) ($S_{Cu} = {}^1/_2$), there are three exchange coupled states, namely, $|S_t, S^*\rangle = |{}^1/_2,0\rangle$, $|{}^1/_2,1\rangle$, and $|{}^3/_2,1\rangle$ or pictorially ($\uparrow\uparrow\downarrow$), ($\uparrow\downarrow\uparrow$), and ($\uparrow\uparrow\uparrow$), respectively, in which S_t represents the total spin $S_t = S_{Cu} + S_{R1} + S_{R2}$ and the subspin $S^* = S_{R1} + S_{R2}$. Thus, the systems can be described by the isotropic exchange Hamiltonian

$$H = -2J(S_{R1} \cdot S_{Cu} + S_{Cu} \cdot S_{R2}) - 2J_R(S_{R1} \cdot S_{R2})$$

in which J represents the copper-radical and J_R the radical−radical interactions. Hence, the relative order of the spin states $|S_t,S^*\rangle$ depends on the sign and magnitude of two exchange interactions, J and J_R. As the simulation of the experimental magnetic data by using the Hamiltonian given above results in correlated J and J_R values, EPR spectroscopy was very helpful to determine which of the two doublets $|{}^1/_2,0\rangle$ or $|{}^1/_2,1\rangle$ constitutes the ground state for complexes **1**−**5**. EPR results at low temperatures indicate that the ground spin state has predominant copper(II) character; as a repre-

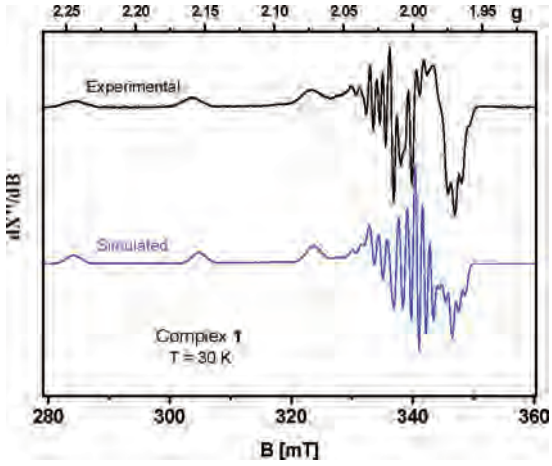

Figure 3. X-band EPR spectrum of **1** in CH_2Cl_2, measured at 30 K. Conditions: microwave frequency 9.637 GHz, microwave power 0.01 mW, modulation amplitude 3.0 G.

Table 4. Simulated Parameter Obtained from the EPR Spectra for **1**−**6**

complex	g_1	g_2	g_3	A_{Cu} (10^{-4} cm^{-1})	A_N (10^{-4} cm^{-1})
1 (−CF_3)	2.058	2.03	2.197	(2,5,580)	(43,33,25)
1a (−$2CF_3$)	2.006	2.005	2.24	(20,10,160)	
2 (−F)	2.065	2.026	2.198	(20,20,580)	(37,50,30)
3 (−Cl)	2.068	2.023	2.208	(30,30,580)	(45,40,15)
4 (−OCH_3)	2.059	2.02	2.195	(2,5,570)	(40,50,20)
5 (−^{t}Bu)	2.06	2.03	2.19	(2,5,555)	(43,33,25)
6 (−H)[a]	2.06	2.03	2.20	(0,18,188)	

[a] Reference 7.

sentative of the spectra the EPR spectrum of **1** in CH_2Cl_2 at 30 K is shown in Figure 3 together with its simulation with $g_1 = 2.058$, $g_2 = 2.03$, $g_3 = 2.197$, $|A_{Cu}| = (2,5,580) \times 10^{-4}$ cm^{-1}, $|A_N| = (43,33,25) \times 10^{-4}$ cm^{-1}. The g values and hyperfine data are fully compatible with those expected for Cu(II) complexes with a $(d_{x^2-y^2})^1$ ground state. The EPR-parameters for all complexes **1**−**5** are listed in Table 4. Thus, it appears that the antiferromagnetic radical−radical interactions J_R dominate over the copper-radical interactions, J, in all distorted planar complexes **1**−**6** of our study, and consequently the exchange interactions lead to an almost "isolated" Cu(II) spin character of the ground state. The experimental spectrum of **1**, shown in Figure 3, and the EPR spectra of **1a**, **2**−**5** clearly establish $g_{||} > g_{\perp}$, and hence a $|^1/_2,0\rangle$ ($\uparrow\uparrow\downarrow$) ground state prevails in complexes **1**−**5** because of the dominating antiferromagnetic coupling between the radical anions, similar to that reported for **6** earlier.[7]

Thus, with the constraint that $|J_R| - |J|$ is large, we have simulated the magnetic data by keeping $J = 0$ (fixed) and the solid lines in Figure 2 represent such simulations with a single effective coupling constant, which we designate J'_R. During the simulations we have kept $g_R = 2.00$ (fixed) and used g_{Cu} values evaluated from the EPR measurements (Table 4). The fitting parameters are listed in Table 5. We do not claim that the values for J_R derived from such simulations are accurate, but they do demonstrate that the coupling between the radical anions is antiferromagnetic in nature and its strength depends on the nature of the substituents of the aniline moiety. Nesting of the μ_{eff} versus T-plots at $T > 200$ K is a clear indication of the small but significant variation of the coupling constants with the various substituents,

Table 5. Variation of Effective Radical-Radical Coupling Constants J'_R as a Function of the Substituents on the Aniline-Moiety in Complexes **1**−**5**

complex	**1**	**1a**	**2**	**3**	**4**	**5**	**6**
J'_R/cm^{-1}	−340	−390	−350	−330	−370	−450	−400[b]
g_{Cu} (fixed)[a]	2.096	2.086	2.097	2.101	2.092	2.095	−

[a] From Table 4: $g_{Cu} = (\sum g_i^2/3)^{1/2}$. Constraints used: $J = 0$ (fixed), $g_R = 2.00$ (fixed). [b] Reference 7.

Scheme 3

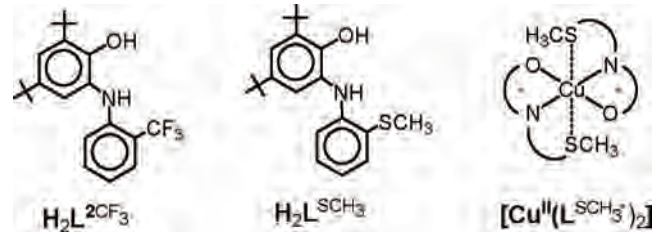

although a univocal magnetic trend is complicated by the fact that the structural factors couple with the inductive effects of the aniline substituents.

At this point a comparison of the magnetic properties of **1**−**6** with those of a very similar copper(II)-diradical complex is warranted. Recently Kaim et al. reported[28] the following interesting compound, $[Cu^{II}(L^{SCH_3\bullet})_2]$, where the ligand $[L^{SCH_3\bullet}]^-$ contains a methylthioether, $-SCH_3$, substituent at the position 2 of the aniline moiety and is very similar to our complex **1a**, $[Cu(L^{2CF_3\bullet})_2]$, which is devoid of the potential thioether ($-SCH_3$) donor atom (Scheme 3).

In contrast to **1**−**6**, complex $[Cu^{II}(L^{SCH_3\bullet})_2]$ exhibits the ground state $|^1/_2,1\rangle$ ($\uparrow\downarrow\uparrow$), because of dominating copper-radical interactions over the radical−radical interactions. This contrasting behavior has been attributed by the authors[28] to the dihedral angle of 32.2° between the two Cu-planes N1CuO1/N2CuO2 of $[Cu(L^{SCH_3\bullet})_2]$. It is noteworthy, that complexes **1** and **1a** with the dihedral angles 24.2° and 25.4° (Table 3), respectively, also exhibit twisted copper coordination environments, but with the spin alignment $|^1/_2,0\rangle$ ($\uparrow\uparrow\downarrow$) as the ground state. Probably the additional weak Cu^{II}−S (thioether) interactions [3.198(1) Å, and 3.475(1) Å][28] in conjunction with the tetrahedral distortion bring the d_{z^2} orbital in play in $[Cu^{II}(L^{SCH_3\bullet})_2]$, thus increasing the metal-radical interactions.

Computed Spin Coupling Scheme. All experimental evidence indicates that the electronic ground state of **1** is of doublet spin multiplicity ($S = {}^1/_2$). The existence of a BS UKS DFT solution, however, supports the notion that an unusual spin coupling scheme might operate in **1**. We have obtained this spin coupling scheme by determining the magnetic orbitals for the BS state of **1**. By applying rules (i) and (ii) outlined in the Experimental Section, we have determined the magnetic orbitals for **1**. On the basis of this overlap-oriented selection procedure, we conclude that α-MO 170, β-MO 169, and β-MO 131 are the magnetic orbitals for the BS ground state of **1**. These MOs are represented in Figure 4 by drawing isosurface values of 0.05.

The α-MO 170 (top left) in Figure 4 is a π-MO localized

(28) Ye, S.; Sarkar, B.; Lissner, F.; Schleid, T.; van Slageren, J.; Fiedler, J.; Kaim, W. *Angew. Chem., Int. Ed.* **2005**, *44*, 2103.

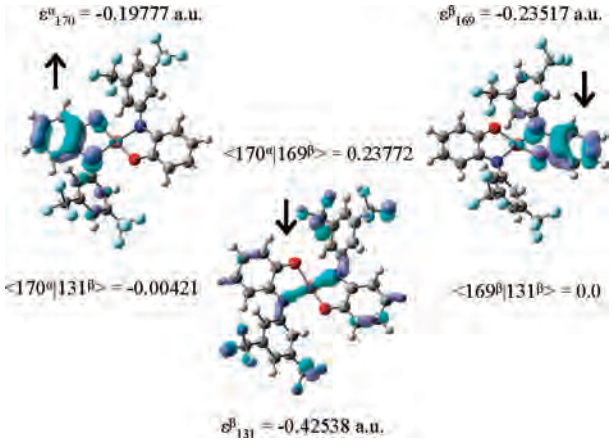

Figure 4. Magnetic orbitals α-MO 170, β-MO 169, and β-MO 131 of complex **1** are illustrated with isosurface values of 0.05. The resultant spin coupling scheme is indicated by the bold black arrows.

at the left ligand. The β-MO 169 (top right) is also a π-MO, but situated at the right-hand ligand. The β-MO 131 (bottom) is of σ-symmetry and predominantly localized at the central copper atom and the trans-oriented ligand nitrogens. Both π-MOs appear with higher energy than the σ-MO as indicated by the Kohn−Sham eigenvalues $\varepsilon^{\alpha(\beta)}$. The shape of the magnetic orbitals (Figure 4) suggests the following spin coupling operating in **1**. The opposite spins of the two electrons localized in α-MO 170 and β-MO 169 are strongly antiferromagnetically coupled. The left over uncoupled β-spin electron in β-MO 131 determines the overall doublet spin multiplicity of the electronic ground state of **1**. The shape of β-MO 131 shows that the unpaired β-spin electron is mainly localized at the copper atom. This spin localization, found by theory alone, is in accord with the EPR experiments. The β-MO 131 extends also toward the nitrogen atoms of **1** (Figure 4). Thus, a small amount of spin density should be present at the nitrogen atoms. This finding is again supported by the EPR measurements of **1**. The overlap integral between α-MO 170 and β-MO 169 is 0.238. A significantly smaller value of −0.004 is computed for α-MO 170 and β-MO 131. The overlap integral between β-MOs 169 and 131 is exactly zero based on the fact that all MOs of the α- or β-MO set of an UKS Slater determinant[29] are orthonormal. Thus, the overlap integrals support the suggested spin coupling scheme and they are in line with the Goodenough−Kanamori rules.[30] The overlap integrals show that the antiferromagnetic spin coupling of the electrons situated in α-MO 170 and β-MO 169 is predominant. The β-spin of the electron in β-MO 131 remains almost uncoupled. The two magnetic β-MOs are orthogonal. Consequently, a ferromagnetic coupling is expected for the interaction of the two electrons of β-spin. The magnetic α-MO 170 and β-MO 169 are the highest occupied Kohn−Sham orbitals of the α- and β-MO set, respectively. This finding and the shape of the two MOs (Figure 4) corroborate the notion that *electrochemical* redox processes (loc. cit.) of **1** are ligand-centered and that the ligand-π system is involved

(29) Slater, J. C. *Phys. Rev.* **1930**, *36*, 57.
(30) (a) Goodenough, J. B. *Phys. Rev.* **1955**, *100*, 564. (b) Kanamori, J. *J. Phys. Chem. Solids* **1959**, *10*, 87.

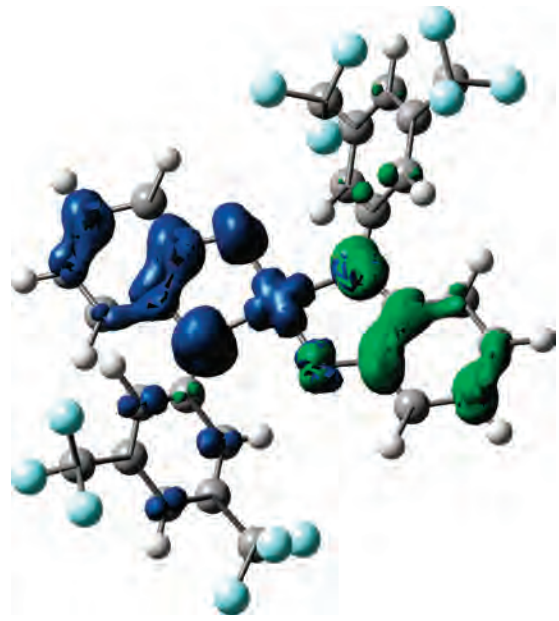

Figure 5. Computed spin density distribution, plotted with isosurface values of 0.005, for complex **1**. Blue and green surfaces indicate α- and β-spin populations, respectively, resulting in the spin coupling scheme R-Cu-R(↑↑↓).

in the uptake and donation of electrons.

The magnetic orbitals represented in Figure 4 should also determine the spin density distribution in **1**. This spin density distribution is shown in Figure 5.

The spin density is based on the UKS Slater determinant for the BS DFT solution ($\langle S^2 \rangle = 1.6470$) for **1** that yields the lowest energy. Blue and green surfaces indicate spatial regions where electrons with α- and β-spin prevail, respectively. We realize that the spin density distribution for **1** indicates a spin coupling scheme of the type Ligand ↑-Cu↑-Ligand ↓. This is the spin coupling scheme suggested by the magnetic orbitals depicted in Figure 4. Thus, the theoretical results match well with the experimental findings.

Electro- and Spectroelectrochemistry and EPR Spectra of the Electrogenerated Species. CVs of all complexes have been recorded in CH_2Cl_2 solutions containing 0.10 M $[(n\text{-}Bu)_4N]PF_6$ as supporting electrolyte at a glassy carbon working electrode and a $Ag/AgNO_3$ reference electrode. Ferrocene was used as an internal standard, and potentials are referenced versus the ferrocenium/ferrocene couple (Fc^+/Fc). The CVs of all complexes are very similar and exhibit four reversible one-electron transfer waves, of which, according to coulometric measurements, two correspond to oxidations and two to reductions. The redox potentials are similar, and spectroscopic measurements are in line with ligand-centered redox processes; the redox potentials are summarized in Table 6, where ox_1 and ox_2 correspond to first and second oxidation potentials, respectively, and successive reduction potentials are represented by red_1 and red_2. The CV of **1** recorded in the potential range +1.0 to −1.50 V versus Fc^+/Fc is typical for all other complexes and is displayed in Figure 6.

It is clear from Table 6 that the inductive effects (σ effect) of the substituents on the aniline moiety have an effect on the redox potentials; *tert*-butyl groups exhibit +I effect

Table 6. Formal Electrode Potentials for Oxidation and Reduction (in V vs Fc^+/Fc) of Complexes **1**−**6**[a]

complex (substituent)	$E_{1/2}(ox_2)$	$E_{1/2}(ox_1)$	$E_{1/2}(red_1)$	$E_{1/2}(red_2)$
1 (3,5-CF_3)	+0.41	−0.06	−0.804	−1.07
1a (2-CF_3)	+0.536	−0.132	−0.964	−1.411
1b (4-CF_3)	+0.362	−0.122	−0.841	−1.048
2 (3,5-F)	+0.365	−0.12	−0.99	−1.445
3 (3,5-Cl)	+0.36	−0.11	−0.87	−1.10
4 (3,5-OCH_3)	+0.318	−0.30	−1.043	−1.289
5 (3,5-*tert*-butyl)	+0.47	−0.393	−1.16	−1.51
6[b] (unsubstituted)	+0.37	−0.26	−1.02	−1.32

[a] Measured at Ambient Temperatures in CH_2Cl_2 Solutions Containing 0.1 M $[(n\text{-}Bu)_4N]PF_6$; Scan Rate = 100 mV s^{-1}. [b] Reference 7.

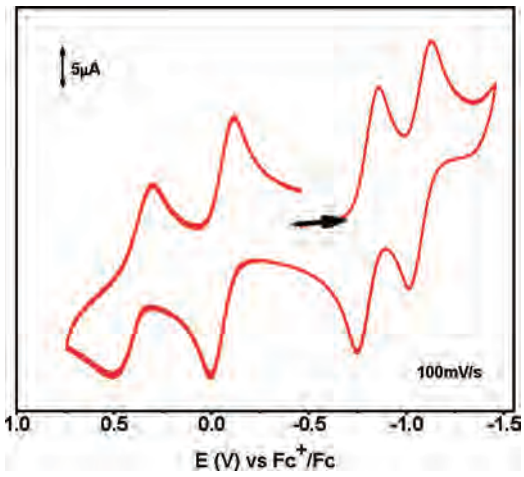

Figure 6. CV of **1** in CH_2Cl_2 at ambient temperature with a scan rate of 100 mV sec^{-1}.

(electron donation), whereas -CF_3 groups show -I effect (electron withdrawing). Thus the electron-donating *tert*-butyl substituents favor easy electron removal, that is, oxidation, as is the case with complex **5** in comparison to complex **1** with the electron-withdrawing CF_3 groups making oxidation difficult. On the other hand, the opposite is expected for reduction processes. Indeed, complex **1** has lower reduction potentials (more positive) than that for complex **5**, which is more difficult to reduce.

Complexes **1**, **1a**, and **1b** with the −CF_3 substituents at different positions behave electrochemically in line with the electron-withdrawing properties of −CF_3: oxidations are impeded but reductions facilitated. As 2-CF_3 group possesses the highest electron-donating capability among the three positions (2- or 4- or 3,5-), complex **1a** shows most easy oxidation.

Theoretical calculations have provided valuable insights for understanding the effect of the meta-substituents on the electrochemical behavior of complex **1**. Let us consider the parent copper complex where substituents in the relevant meta-positions are absent. The electrochemical oxidation is an electron removal from the highest occupied α-MO. This α-MO is depicted in Figure 7 by drawing isosurface values of 0.05.

The MO is preferentially localized at one equatorial ligand and does not extend into the spatial regions of the central copper atom. Thus, an oxidation of the complex should be a ligand centered process. This highest occupied α-MO is a π-MO. Consequently, the oxidation removes a π-electron from the parent complex. The above MO form is characteristic for all MOs of the various meta-substituted derivatives that are involved in the oxidation processes. In some derivatives those π-MOs extend over both equatorial ligands, but functional values at the copper atoms are absent.

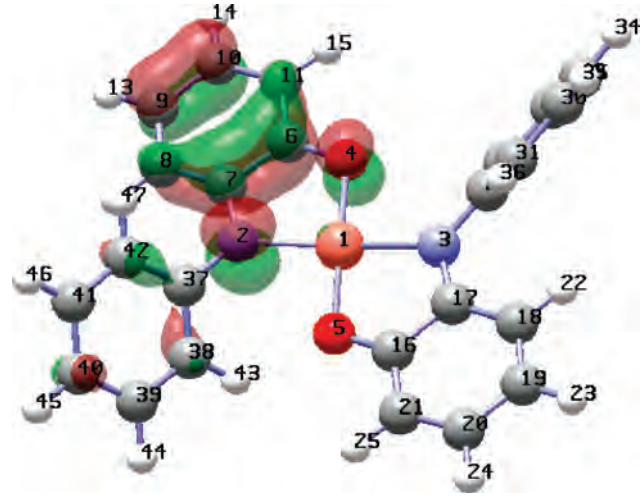

Figure 7. Shape of the HOMO (α-MO) of complex **6** (unsubstituted) indicating its dominating ligand-character (isosurface cutoff value 0.05).

The depicted π-MO (Figure 7) is largely localized at the atoms C_8, C_7, C_6, and C_{11}. If a π-electron in this MO sees a large positive nuclear charge of carbon atoms C_8, C_7, C_6, and C_{11}, the π-electron is tightly bound. Consequently, a large energy is needed to remove the π-electron from this MO. If the π-electron sees a small positive carbon nuclear charge, the electron is only weakly bound. Only a small energy is required to remove the π-electron from this MO. Thus, the effective nuclear charges of carbon atoms C_8, C_7, C_6, and C_{11} (Figure 7) are decisive. If the carbon σ-electrons are close to the nuclei, the carbon nuclear charges are effectively screened, and a small energy is needed to remove the π-electron. If the σ-electrons are further off the nuclei, the carbon nuclear charges are less screened.[31] More energy is needed to remove a π-electron. Let us consider carbon atom C_7 where the π-MO contribution is large (Figure 7). The 2s σ-electrons are well characterized by the natural atomic orbitals (NAOs) and their energies. If the 2s NAO energy is low, the 2s electrons are closer to the carbon nucleus and an effective screening occurs. If the 2s NAO energy is high, the 2s electron is further off the carbon nucleus and the carbon nuclear charge gets less screened. Of course, the here applied reasoning resembles the classic method of Slater to determine effective screening constants for his famous atomic orbitals.[29]

For all meta-substituted derivatives we selected those carbon atoms that correspond to carbon C_7 of Figure 7. In Figure 8, the 2s α-NAO energies of the relevant carbon atoms and the observed oxidation potentials of the meta-substituted derivatives are related.

The existing correlation supports the above outlined reasoning. The various substituents modulate the 2s α-NAO energies and different nuclear charge screenings arise. The different screenings influence the π-electron energies as is

(31) Pilar, F. L. *Elementary Quantum Chemistry*; McGraw-Hill: New York, 1968; pp 193−195.

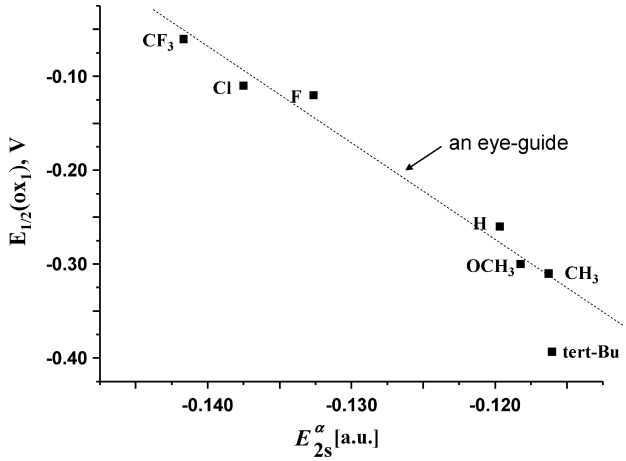

Figure 8. Plot of $E_{1/2}(ox_1)$ for the copper(II)-diradical complexes against the 2s α-NAO energies of the relevant carbon atoms in the meta-substituted derivatives, showing a linear relationship.

reflected by the observed sequence of oxidation potentials. *The obtained correlation supports the notion that substituents in meta-position operate via the σ-electron system.*

The UV−vis/NIR spectra of all complexes are quite similar. Figure 9 displays the spectra of complexes $[Cu^{II}(L_{SQ}{}^{CF_3\bullet})_2]^0$ [**1**], $[Cu^{II}(L_{SQ}{}^{CF_3\bullet})(L_{AP}{}^{CF_3})]^{1-}$ $[\mathbf{1}]^{1-}$, $[Cu^{II}(L_{SQ}{}^{CF_3\bullet})(L_{BQ}{}^{CF_3})]^{1+}$ $[\mathbf{1}]^{1+}$, $[Cu^{II}(L_{AP}{}^{CF_3})_2]^{2-}$ $[\mathbf{1}]^{2-}$, $[Cu^{II}(L_{BQ}{}^{CF_3})_2]^{2+}$ $[\mathbf{1}]^{2+}$ in CH_2Cl_2 solution, and Table 7 contains the results for electronic spectra of all complexes. After controlled potential one-electron reduction, species $[\mathbf{1}]^-$, the band assigned to ligand-to-ligand charge transfer (LLCT) at around 800 nm for **1** diminishes. The ligand (phenoxyl) π-π^* charge transfer band at around 440 nm also diminishes, and a new sharp band at 355 nm (ε = 23000 M^{-1} cm^{-1}) for $[\mathbf{1}]^-$ appears. On further reduction of $[\mathbf{1}]^-$ to $[\mathbf{1}]^{2-}$, the band at 800 nm disappears and a sharp, strong band which can be assigned to ligand-to-metal charge transfer at 378 nm (ε = 37200 M^{-1} cm^{-1}) arises. The band at 656 nm (ε = 900 $^{-1}$ cm^{-1}) might be due to the d-d transition of Cu(II)(d^9) ion.[32] Upon controlled potential one-electron oxidation, the band around 800 nm for **1** decreases in intensity and two new bands at 635 nm (ε = 11800 M^{-1} cm^{-1}) and at 460 nm (ε = 7600 M^{-1} cm^{-1}) appear for $[\mathbf{1}]^+$. The band at 635 nm can be assigned to an intervalence LLCT band and the shift of the band to the lower wavelength region could be due to increase of metal−ligand interaction in the mono positive species, $[\mathbf{1}]^+$, ($[Cu^{II}(L_{SQ}{}^{CFM_3\bullet})(L_{BQ}{}^{CF_3})]^{1+}$). The band at 460 nm is assigned to π-π^* transition of the iminobenzoquinone moiety. Upon two one-electron oxidations, that is, for $[\mathbf{1}]^{2+}$, sharp and strong band assigned to π-π^* of the iminobenzoquinone moieties appears at 510 nm (ε = 5900 M^{-1} cm^{-1}) and the assigned intervalence LLCT band disappears totally.

All neutral complexes consist of three paramagnetic centers: two radicals and one copper(II) (d^9) center. Variable-temperature magnetic susceptibility measurements discussed earlier have shown that all complexes acquire an $S_t = {}^1/_2$ ground state. Hence, the ground-state electronic configuration can be either (↑↓↑) [R-Cu-R] or (↑↑↓) [R-Cu-R]. In the first case the radical centered EPR spectrum is expected whereas the copper(II) (d^9) centered EPR spectrum should be observed if the antiferromagnetic coupling between two radicals dominates.

Electrochemically generated one-electron oxidized and one-electron reduced species of **1**, symbolically $[\mathbf{1}]^{1+}$ and $[\mathbf{1}]^{1-}$, are X-band EPR silent. Both two-electron oxidized and two-electron reduced species, symbolically $[\mathbf{1}]^{2+}$ and $[\mathbf{1}]^{2-}$, are EPR active; EPR characterization of the oxidized and reduced species yielded anisotropic spectra at low temperatures implying that the unpaired electron has significant metal-based character. Figures 10 and 11 show the EPR spectra of $[\mathbf{1}]^{2+}$ and $[\mathbf{1}]^{2-}$, respectively. These spectra support further the notion that the redox processes of complex **1** are ligand-based. Thus, the electrochemical behavior of **1** can be summarized as shown in Scheme 4.

Catalytic Oxidation of Primary Alcohols by Air. We have examined the catalytic activity of **1**, **2**, **4**, **5**, and **6** for the aerial oxidation of primary alcohols to aldehydes in dichloromethane according to the reaction

$$RCH_2OH \xrightarrow[CH_2Cl_2]{\text{Cat, Air}} RCHO + H_2O_2$$

The reactivity studies were performed in dichloromethane because of the good solubility of the complex (catalyst) as well as of the substrate and of its product. As a base, tetrabutylammonium methoxide was added to deprotonate the substrate at least partly. The above catalytic oxidation does not proceed in the absence of the catalysts, the copper(II)-diradical complexes.

Prior to a detailed kinetic study, we quantitatively evaluated the catalytic activity of the complexes. For this purpose, 1×10^{-5} mol of a complex (catalyst) in 20 mL of dichloromethane was treated with 100 equiv of either (i) benzylalcohol and 1×10^{-5} mol of tetrabutylammonium methoxide, (ii) tetrabutylammonium ethoxide, or (iii) tetrabutylammonium methoxide, and the resulting solution was stirred in air at ambient temperature for 16 h. The products were analyzed for aldehydes by LC, GC, or spectrophotometric methods, and Table 8 summarizes the yields of products for the substrates mentioned.

That for the oxidation of benzyl alcohol to benzaldehyde complexes **1**−**6** are equally efficient as catalysts is evident from Table 8. Together with the major product (∼70%), a small amount of formaldehyde (3−16%) was detected for different complexes because of the presence of the base methoxide added to the substrate benzyl alcohol. Lower C−H bond dissociation energy of benzyl alcohol in comparison to that of methanol (105 vs 124 kcal mol^{-1}, respectively) results in preferable oxidation of benzyl alcohol than that for methanol, as is evident from Table 8.

The oxidation yield of ∼25% for ethanol or methanol (Table 8) can be increased to ∼75−80% by changing the catalyst/substrate ratio to 1:25 instead of 1:100; the results of the latter are shown in Table 8. The lesser yields for complexes **2**−**6** for such oxidations are attributable to the lower stability of the catalysts in the strongly basic catalytic

(32) Thomas, F.; Jarjayes, O.; Duboc, C.; Philouze, C.; Saint-Aman, E.; Pierre, J.-L. *Dalton Trans.* **2004**, 2662.

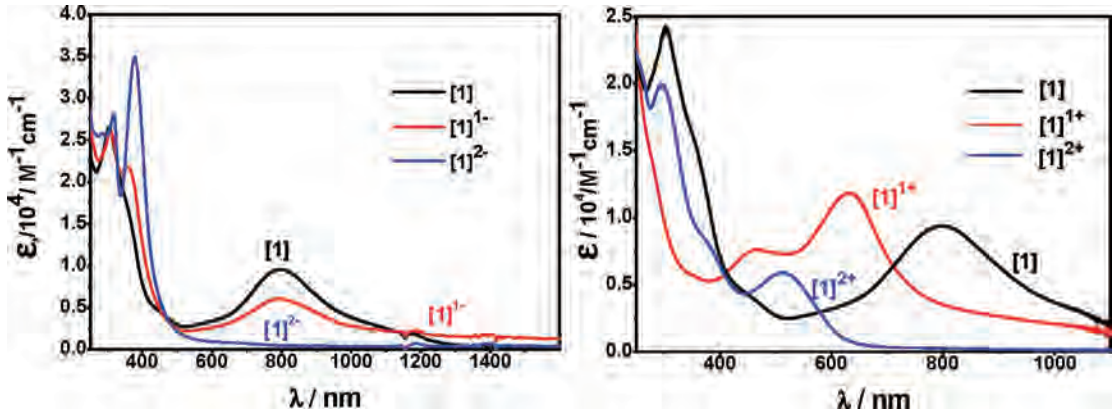

Figure 9. Electronic spectra of complex [**1**] and of the electrogenerated $[\mathbf{1}]^{+}$, $[\mathbf{1}]^{2+}$, $[\mathbf{1}]^{-}$, and $[\mathbf{1}]^{2-}$ in CH_2Cl_2.

Table 7. Electronic Spectral Data for **1**, **2**, **4**, and **5** Together with Spectroelectrochemical Data for Electrogenerated $[\mathbf{1}]^{-}$, $[\mathbf{1}]^{2-}$, $[\mathbf{1}]^{+}$, and $[\mathbf{1}]^{2+}$ Species[a]

complex	λ, nm (ε, M^{-1} cm^{-1})
1	440sh(5170), 800(10200), 1040sh(3300)
$[\mathbf{1}]^{-}$	355(23000), 790(6500)
$[\mathbf{1}]^{2-}$	378(37200), 656(900)
$[\mathbf{1}]^{+}$	460(7600), 635(11800)
$[\mathbf{1}]^{2+}$	510(5900)
2	435(4720), 797(7700), 1100sh(2180)
4	456(5400), 791(6650), 1085sh(2570)
5	350(21500), 450(10500), 780(8200), 1050(4000)

[a] Solvent = Dichloromethane, Temperature = 22 ± 1 °C, Sh = Shoulder.

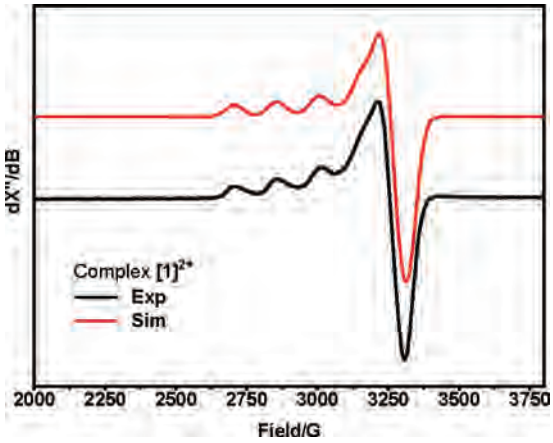

Figure 10. X-band EPR spectrum of complex $[\mathbf{1}]^{2+}$ in CH_2Cl_2 solution at 10 K under argon atmosphere. Simulated parameters: $g_1 = g_2 = 2.065$, $g_3 = 2.30$, $A_z = 160 \times 10^{-4}$ cm^{-1}.

solutions.

We could not detect any oxidation product (acetone or C−C products) in the case of isopropanol as the substrate, implying that complexes **1**−**6** do not act as catalysts for the aerial oxidation of secondary alcohols.

As complex **1** appeared to be the best catalyst among complexes **1**−**6** for the aerial oxidation of primary alcohols, the kinetic studies using the initial rate method were performed with complex **1** by using the spectrophotometric methods for determining the concentrations of formaldehyde or acetaldehyde with time. The formation of formaldehyde or acetaldehyde was further verified by chromatographic (GC, GC-MS) and mass spectroscopic (EI, ESI) methods of the Schiff-base products originated from 2,4-dinitrophenylhydrazine or 3-methyl-2-benzothiazolone hydrazine as aldehyde-capturing reagent. We have measured the kinetics of the oxidative catalysis at 22 ± 1 °C in CH_2Cl_2 by varying the concentration of the catalyst in the range of 1.25×10^{-4} to 10×10^{-4} M and that of the substrate in the range of 6×10^{-3} to 4.5×10^{-2} M. From the experimental rate constants with $k_{cat} = 6.1 \times 10^{-4}$ sec^{-1} and $k_{sub} = 1.6 \times 10^{-5}$ sec^{-1}, an overall rate-law was deduced:

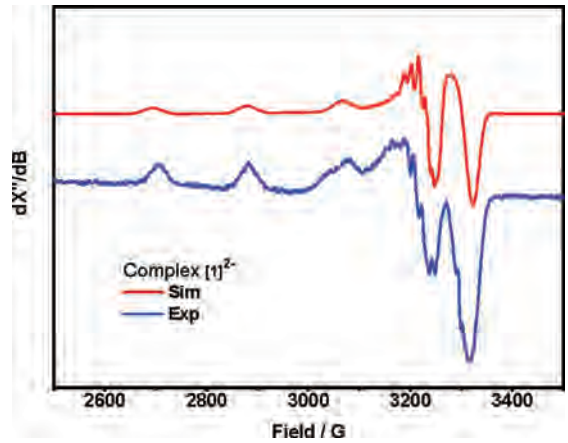

Figure 11. X-band EPR spectrum of complex $[\mathbf{1}]^{2-}$ in CH_2Cl_2 solution at 80 K under argon atmosphere. Fitting parameters: $g_1 = 2.048$, $g_2 = 2.065$, $g_3 = 2.23$, $A_i = (2,20,162) \times 10^{-4}$ cm^{-1}, $A_N = (6,12,3) \times 10^{-4}$ cm^{-1}.

$$\text{Rate} = k[\text{Complex } \mathbf{1}][\text{Alcohol}]$$

The observed first-order dependence of the rate on complex **1** (catalyst) and on the substrate (alcohols) indicate the composition of the activated complex; in other words, one molecule of complex **1** is utilized for the two-electron oxidation of one molecule of alcohols.

To shed more light on this two-electron oxidation process, we performed additional experiments to demonstrate the following salient points: (i) the radicals coordinated to the Cu(II)-center in **1** are participating in the redox process; (ii) oxygen of air is essential for the catalysis; and (iii) H-atom abstraction is involved in the rate-determining step.

The kinetics of the oxidation of methoxide to formaldehyde using the deuterated substrate CD_3O^{-} have been measured and the change in the concentration of formaldehyde with time is shown for both CH_3O^{-}- and CD_3O^{-}-substrates in Figure 12.

Scheme 4. Electrochemically Generated Different Redox States for Complex **1**

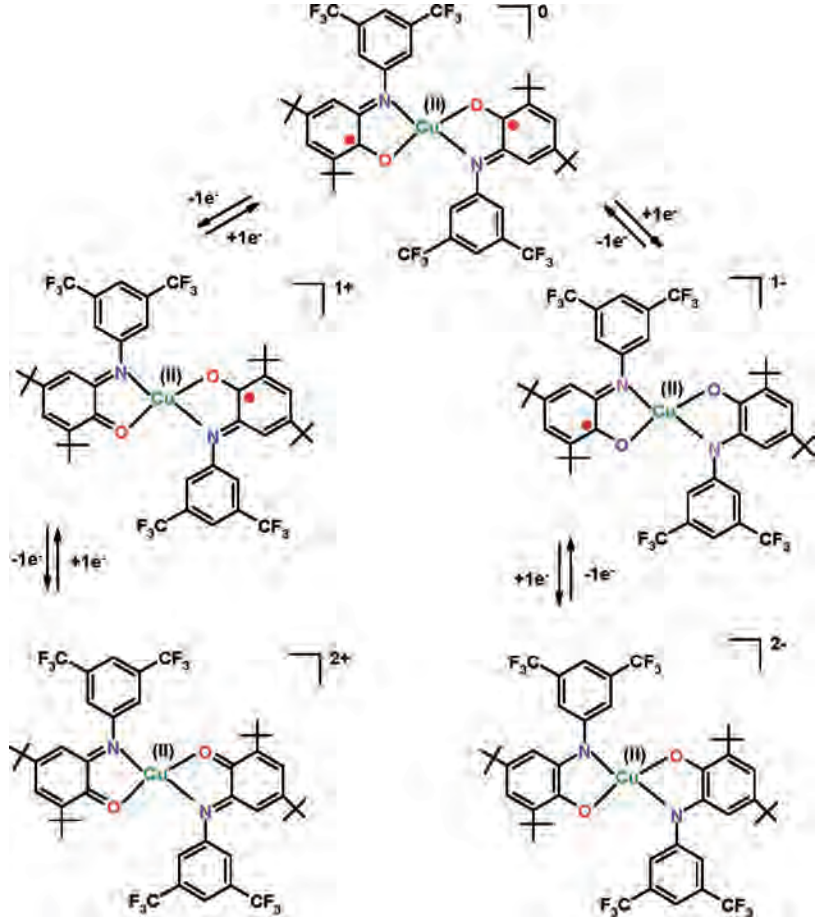

Table 8. Yields of the Aldehydes Observed After Aerial Oxidation of Benzyl Alcohol, Ethanol, and Methanol

complex	C_6H_5CHO (%)	CH_3CHO (%)	HCHO (%)
1 (3,5-CF_3)	72	25	25
2 (3,5-F)	63	~10	16
4 (3,5-OCH_3)	68		10
5 (3,5-*tert*-butyl)	69		10
6 (unsubstituted)	70		10

The k_H/k_D ratio of ~5 (Figure 12) indicates a small but significant primary kinetic isotope effect (KIE) and is a clear indication that hydrogen-atom abstraction from the α-carbon atom of the coordinated alcoholate is the rate-determining step. The resulting ketyl radical, known to be a strong one-electron reductant, is converted to aldehyde via an intramolecular electron-transfer step (see the mechanistic proposal, Scheme 5).

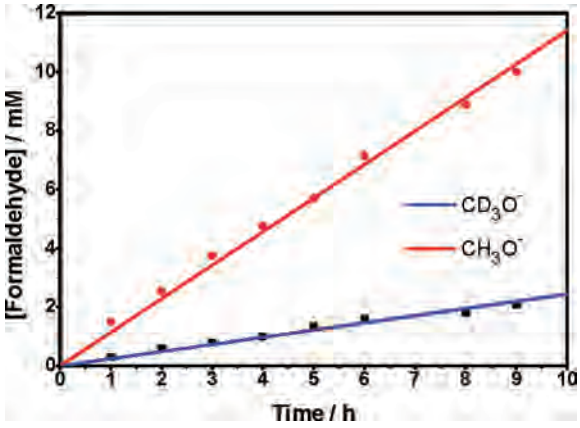

Figure 12. Plots for change in concentration of formaldehyde with time to evaluate the KIE.

When a solution of complex **1** in dry CH_2Cl_2 was added to a 12.5-fold excess of methoxide under argon in a glovebox at ambient temperature, the original blue-green color changed to yellow within a minute. An aliquot of this reaction solution was divided into several parts to (i) determine spectrophotometrically, strictly under argon, the amount of formaldehyde formed in absence of air, (ii) measure the concentration of hydrogen peroxide, extracted into an aqueous phase from the reaction solution by the titanyl sulfate reagent, (iii) measure an EPR spectrum, and (iv) record the UV−vis/NIR spectrum of the reaction solution from the glovebox.

From the quantitative spectrophotometric study, strictly under argon, the formation of only 1 equiv of formaldehyde could be observed, indicating that two electrons of **1** are involved. It has been shown by electrochemistry that the two reversible reduction processes are ligand centered, which occur before the metal-centered reductions. Hence, for the oxidative catalytic process, reductions of two radical centers are conceivable. The overall first step in the process can then be summarized as

$$[Cu^{II}(L^{CF_3}\bullet)_2]^0 + CH_3O^- \xrightarrow{\text{Argon}} [Cu^{II}(L^{CF_3}{}_{AP})_2]^{2-} + HCHO + H^+$$

Figure 13 shows the UV−vis/NIR spectrum of the reaction solution under argon, which corresponds to that of [Cu^I-

Scheme 5. Proposed Mechanism for the Oxidation of Primary Alcohols by Catalyst **1**

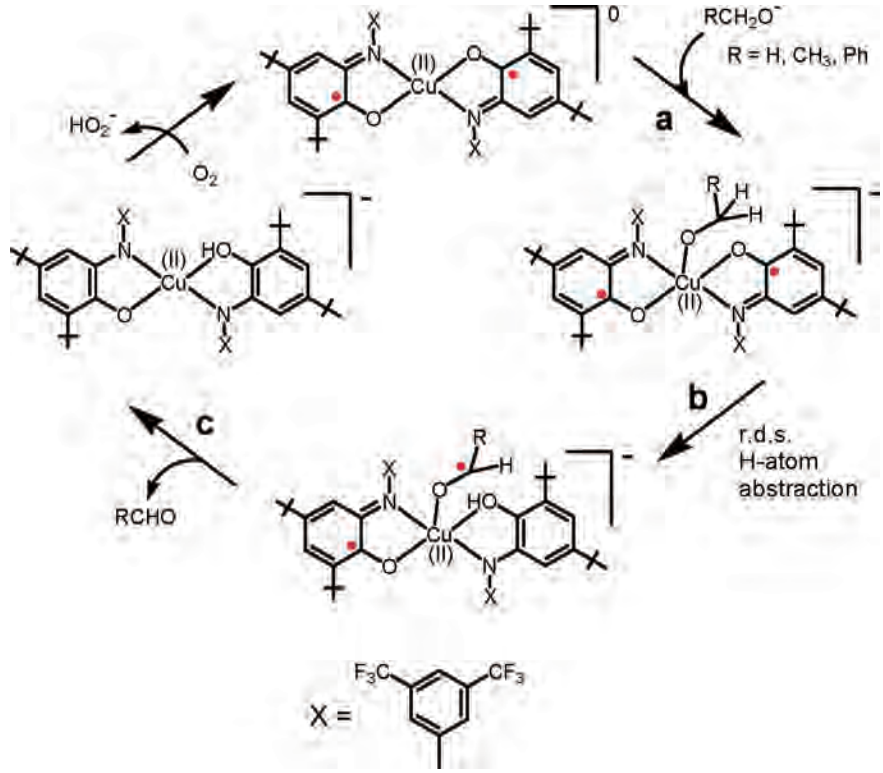

$_{I}(L_{AP}^{CF_3})_2]^{2-}$ generated electrochemically (Figure 9). Subsequently during exposure of the yellow solution to air, a band at 800 nm (LLCT) arises (Figure 13) thus indicating the regeneration of ligand radicals, originally present in the catalyst (complex **1**). Thus, investigations depicted in Figure 13 indicate the essentiality of aerial oxygen and the participation of radicals for the catalytic redox process. The participation of both radicals in the catalytic process is also substantiated by comparing the EPR spectrum of the reaction solution under argon with that of the species $[\mathbf{1}]^{2-}$, obtained from the two-electron electrochemical reduction of complex **1** (Figure 11); they are identical. Thus, the regeneration of the catalyst can occur in the following way

$$[Cu^{II}(L_{AP}^{CF_3})_2]^{2-} + O_2 \rightarrow [Cu^{II}(L_{SQ}^{CF_3\bullet})_2]^{0} + O_2^{2-}$$

The presence of hydrogen peroxide in the catalytic solution could not be detected either by the titanyl(iv) sulfate reagent or by the liberation of iodine from an acidic potassium iodide solution, presumably because of the decomposition of formed hydrogen peroxide to H_2O and O_2. Moreover, because of the sluggish nature in the reaction, even at lower temperatures, for example, at −25 °C, it was not possible to detect or determine H_2O_2 (concentration), which decomposes at a much faster rate in the prevailing strongly basic medium. The extremely slow nature of the oxidation also prevented us from examining the O_2-uptake measurements accurately.

On the basis of the kinetic and electrochemical data and the anaerobic experiments described earlier, it is tempting to propose a mechanism involving stepwise pathways,

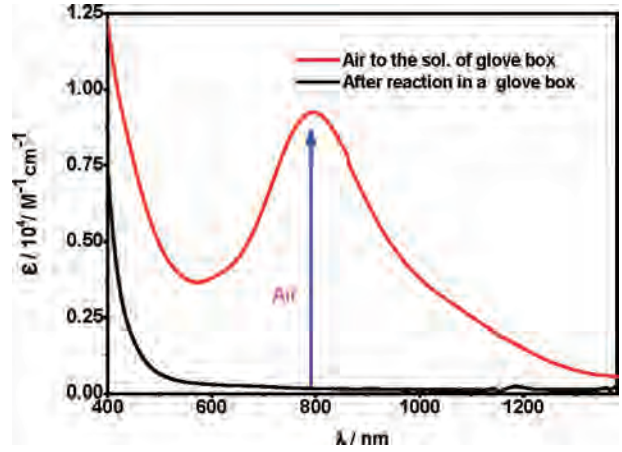

Figure 13. Electronic spectra of the reaction solution obtained from the glovebox (black line) and of the solution after its exposure to air (red line).

keeping in mind that it is impossible to prove any single mechanism. A tentative catalytic cycle for the oxidation of primary alcohols is shown in Scheme 5.

The first step (**a**) is the coordination of an alcoholate ligand to the catalyst, **1**, which is followed by the rate-determining H-atom transfer from the α-C atom of the bound alcoholate, in which a coordinated ketyl radical anion results. An intramolecular electron transfer through the copper(II)-center yields the two-electron reduced species $[Cu^{II}(L_{AP}^{CF_3})_2]^{-}$ (**c**) and the product aldehyde leaves the cycle. The catalyst **1** is regenerated by aerial oxygen.

The protonated two-electron reduced catalyst$[Cu^{II}(HL_{AP}^{CF_3})_2]^{-}$ (step **c**, Scheme 5) is favored by us over its valence-tautomer involving Cu(I)-radical species, as the necessarily enforced planar geometry for the Cu(I)-form is generally uncommon.

Obviously rapid dissociation of the protonated form from the copper(I)-radical center making the center 3-coordinated is also a possibility. Our observations of an anisotropic EPR spectrum (Figure 11) (i.e., absence of a radical) and absence of any intense visible band (Figure 13) of the catalytic solution under argon support the analysis. Regeneration of the catalyst invokes participation of O_2, presumably resulting in the formation of an intermediate bicyclic endoperoxide species involving the fully reduced form of the ligand AP, the amidophenolate anion, and copper(II). Such an endoperoxo species formed by O_2 binding to a very similar amidophenolate antimony(V) center has been reported recently.[33]

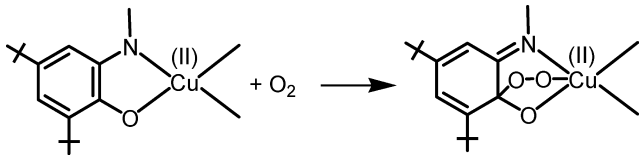

With our preliminary mechanistic data at hand, particularly without a concrete knowledge of catalyst/O_2 stoichiometry, we have considered here only one of the different mechanistic possibilities.[34]

Concluding Remarks

To conclude, the following points of this study deserve particular attention.

As an obvious progression of our earlier reports,[7−15] a series of disubstituted 2-anilino-4,6-*tert*-butylphenol ligands have been used to synthesize seven new diradical-containing copper(II) compounds. As expected, the effective antiferromagnetic radical−radical interactions dominate over the copper(II)-radical interactions, resulting in an $S_t = {}^1/_2$ ground state attributable to an almost "isolated" copper(II) spin character. The spin-coupling scheme R-Cu-R(↑↑↓) obtained from BS DFT complements the experimental findings. A clear indication of the small but significant variation of the coupling constants with the various substituents has been observed.

Electrochemical measurements indicate four reversible redox processes that are ligand centered. Thus, two oxidations resulting in the quinone forms and two reductions resulting in the amidophenolate forms of the ligands are discernible. Theoretical calculations (DFT) have provided valuable insights for understanding the effect of the meta-substituents on the electrochemical behavior of the complexes. A correlation between 2s α-NAO energies of the relevant carbon atoms in the meta-substituted derivatives of the complexes and the observed $E_{1/2}(ox_1)$ potentials supports the notion that the meta-substituents operate via the σ-electron system.

The investigation emphasizes that the copper(II)-diradical complexes **1**−**6** can catalyze the oxidation of primary alcohols with aerial oxygen as the sole oxidant to afford aldehydes in good yield under mild conditions to mimic the function of the copper-containing enzyme Galactose Oxidase (GO).

$$RCH_2OH \xrightarrow[\text{Complexes } \mathbf{1}\text{–}\mathbf{6}]{\text{Air, } CH_2Cl_2} RCHO$$

Although the nature of the substituents on the aniline moiety of the ligand causes a shift of the reversible redox potentials in the expected manner, that is, electron-withdrawing groups facilitate the reductions and impede the oxidations and vice versa, this change in potentials is not reflected in the GO-activity, thus indicating that the structural factors couple with the inductive effects of the aniline substituents in complexes **1**−**6**.

A ligand-derived redox activity without apparent participation of the metal center has been proposed for the catalytic process (Scheme 5) in which hydrogen-atom abstraction, evidenced by the presence of kinetic isotope effect (KIE), has been proposed to be the rate-determining step. Complexes containing redox-active "non-innocent" ligands, such as **1**−**6**, are largely unexplored for redox transformations of small molecules, for example, for oxidases-like reactivity. Thus, such redox-active ligands could also be applied to other transition metals, which would allow for a variety of catalysis and spin coupling possibilities, and hence suggesting a future direction for producing new bioinspired catalysts based on these metal-radical motifs.

Acknowledgment. Financial support from the Max-Planck-Society and German Research Council (DFG) is gratefully acknowledged (Project: Priority Program "Radicals in Enzymatic Catalysis", SPP 1071: Ch111/2-3). Our thanks are also due to Biplab Biswas for some EPR-simulations.

Supporting Information Available: Details of the X-ray structural data for **1a**, **2**−**5** and X-ray crystallographic data (CIF), ORTEP diagrams of the neutral molecules **1a**, **2**−**5** shown in Figures S1−S5, respectively. This material is available free of charge via the Internet at http://pubs.acs.org.

IC8009767

(33) (a) Abakumov, G. A.; Poddel'sky, A. I.; Grunova, E. V.; Cherkasov, V. K.; Fukin, G. K.; Kurskii, Y. A.; Abakumova, L. G. *Angew. Chem., Int. Ed.* **2005**, *44*, 2616. (b) Cherkasov, V. K.; Abakumov, G. A.; Grunova, E. V.; Poddel'sky, A. I.; Fukin, G. K.; Baranov, E. V.; Kurskii, Y. V.; Abakumova, L. G. *Chem.—Eur. J.* **2006**, *12*, 3916.

(34) (a) Mirica, L. M.; Ottenwaelder, X.; Stack, T. D. P. *Chem. Rev.* **2004**, *104*, 1013. (b) Lewis, E. A.; Tolman, W. B. *Chem. Rev.* **2004**, *104*, 1047.